

# Ionospheric electron density profiling and modeling of COSMIC follow-on simulations

L.-C. Tsai<sup>1,2</sup> · S.-Y. Su<sup>1</sup> · C. H. Liu<sup>3</sup> · S. Tulasi Ram<sup>4</sup>

Received: 20 May 2015 / Accepted: 24 September 2015 / Published online: 22 October 2015  
© Springer-Verlag Berlin Heidelberg 2015

**Abstract** The FormoSat-3/ Constellation Observing System for Meteorology, Ionosphere and Climate (FS3/COSMIC) has been proven a successful mission on profiling ionospheric electron density ( $N_e$ ) using the radio occultation (RO) technique. A follow-on program (called FS7/COSMIC2) is now in progress. The FS3/COSMIC follow-on mission will have six 24°-inclination and 550-km low Earth orbiting (LEO) satellites and six 72°-inclination and 750-km LEO satellites to receive Tri-G (GPS, GLONASS, and Galileo) satellite signals. FS7/COSMIC2 RO observations were simulated in this study by calculating limb-viewing GNSS-to-LEO TEC values separately through two independent ionospheric models (the TWIM and NeQuick models). We propose a compensatory Abel-inversion scheme to improve vertical  $N_e$  profiling and three-dimensional (3D)  $N_e$  modeling in this FS7/COSMIC2 simulation study with future real observations. In this FS7/COSMIC2 feasibility study the number of RO observations will increase of around 10 times compared with FS3/COSMIC, and the windowing day number to collect  $N_e$  profiles and to derive every half-hour 3D  $N_e$  model could be decreased from 30 to 3 days. The results show that the root-mean-square (RMS) foF2 and hmF2 difference improvements are 46 % (32 %) and 21 % (4.6 %), respectively, in relative percentage over the standard Abel inversion at the TWIM-background (NeQuick-

background) simulation experiment. The RMS modeling errors are about one order less than those from FS3/COSMIC simulations.

**Keywords** Radio occultation observation · FS7/COSMIC2 · Ionospheric  $N_e$  profiling · Ionospheric  $N_e$  modeling

## 1 Introduction

From 1995 to 1997 the University Corporation for Atmospheric Research (UCAR) organized a proof-of-concept experiment on a 735-km low Earth orbiting (LEO) satellite (MicroLab-1 satellite) to receive multi-channel Global Positioning System (GPS) signals and demonstrate active limb sounding of the Earth's neutral atmosphere and ionosphere using radio occultation (RO) techniques (Kursinski et al. 1997; Rocken et al. 1997; Hajj and Romans 1998) as the GPS/Meteorology (GPS/MET) program. After the GPS/MET mission further missions launched with GPS occultation receivers onboard included the Danish Ørsted, the German Challenging Minisatellite Payload (CHAMP), the Argentinean Satellite de Aplicaciones Científicas-C (SAC-C), the U. S.-German Gravity Recovery and Climate Experiment (GRACE), the South African SUNSAT, the Ionosphere Occultation Experiment (IOX), the Taiwanese-American FS3/COSMIC, the MetOp-A, and the Communications/Navigation Outage Forecasting System (C/NOFS). The scientific payoffs from occultation data are enormous, covering disciplines from meteorology (Cucurull et al. 2007) and climatology (Leroy et al. 2006; Borsche et al. 2007) to ionospheric physics (Pi et al. 2009; Tulasi Ram et al. 2009), space weather (Hajj et al. 2000; Yue et al. 2014), and a suite of related Earth science pursuits. Due to the

✉ L.-C. Tsai  
lctsai@csrsr.ncu.edu.tw

<sup>1</sup> Center for Space and Remote Sensing Research, National Central University, Chung-Li, Taiwan, ROC

<sup>2</sup> Institute of Space Science, National Central University, Chung-Li, Taiwan, ROC

<sup>3</sup> Academia Sinica, Taipei, Taiwan

<sup>4</sup> Indian Institute of Geomagnetism, Navi Mumbai, India

success of FS3/COSMIC consisting of six micro-satellites, the joint U.S. and Taiwan RO team, led separately by the National Oceanic and Atmospheric Administration (NOAA) and Taiwan's National Space Organization (NSPO), have decided to move forward with a COSMIC follow-on mission (called FS7/COSMIC2) that will launch six satellites into 24°-inclination and ~550-km orbits in 2016, and another six satellites into 72°-inclination and ~750-km orbits in 2018 (Schreiner et al. 2012; <http://www.nspo.narl.org.tw>). The Global Navigation Satellite Systems (GNSS) RO payload, named Tri-G GNSS Radio-occultation System (TGRS), is being developed by NASA's Jet Propulsion Laboratory (JPL) and will receive multi-channel (1.5 and 1.2 GHz) GPS, GLONASS, and Galileo satellite signals and will be capable of tracking more than 18,000 radio occultation observations per day after both low- and high-inclination constellations are fully deployed. The FS7/COSMIC2 mission will provide nearly an order of magnitude more one-dimensional and near-vertical  $N_e$  profiles.

Compared to other ionospheric remote sensing techniques (bottom side/topside sounding and incoherent scatter), the RO technique has great advantage in unifying near-vertical  $N_e$  profiling with all-altitude capability from the Earth's surface to the LEO satellite orbit altitude and with global coverage, for instance, over oceans and other inaccessible areas. There are two main types of ionospheric  $N_e$  retrieval techniques on RO observations based on different derived measurements: radio bending angle and Slant Total Electron Content (STEC) along the ray-path. In the mid 1960s, a group at Stanford University and the Jet Propulsion Laboratory introduced the Abel inversion technique (Fjeldbo and Eshleman 1969) to recover planet refractivity profiles from observed bending angles induced by the Earth's atmosphere. The Abel inversion has been the foundation of occultation analysis ever since. Applied to GPS RO observations (Kursinski et al. 1997; Hajj and Romans 1998; Schreiner et al. 1999), GPS dual-band phase and calculated Doppler-shift data can be processed to yield ray-path bending angle profiles using the Bouguer's rule and optical geometry properties. Bending angle profiles can be inverted to yield refractive index profiles via the Abel integral transform and then  $N_e$  profiles using the Appleton-Hartree equation. In order to correct the error due to the spherical symmetry assumption on the Abel inversion, Aragon-Angel et al. (2009, 2010) applied the separability concept introduced by Hernández-Pajares et al. (2000) to take  $N_e$  horizontal gradients in ionospheric sounding into account. Another  $N_e$  retrieval technique using RO path TEC data was independently developed by Hajj and Romans (1998) and Schreiner et al. (1999) and was also based on the Abel inversion method but under a straight-line ray propagation assumption. From their studies the corresponding errors from a straight-line propagation assumption are much less than the errors caused by the spheri-

cal symmetry assumption used in the Abel inversion. Applied to the real GPS/MET RO data retrievals, the performance was even better on average because of simple and accurate path TEC measurements that approached a near real-time process. Straus (1999) and Hajj et al. (2000) presented a constrained-gradient Abel inversion method which uses earlier simulated horizontal gradients from other ancillary data (in situ plasma density, nadir-viewing extreme ultraviolet air-glow, and vertical TEC maps derived from ground-based GPS receivers) and constrains the practical Abel inversion considering the horizontal asymmetry effect on  $N_e$  retrieval. Hernández-Pajares et al. (2000) presented another modified Abel inversion algorithm using a separability hypothesis that the ionospheric  $N_e$  can be separated into a vertical TEC function of local time and latitude and another altitude shape function. Wu et al. (2009) defined an asymmetry factor and showed it to be approximately equal to the relative error of retrieved  $NmF2$  and useful to improve retrieved  $N_e$  profiles. Yue et al. (2012) also developed a data assimilation retrieval method to simultaneously assimilate RO observations into an empirical background to provide ionospheric horizontal information and improve ionospheric RO  $N_e$  profiling.

In our earlier investigations, Tsai and Tsai (2004) developed a TEC compensation procedure for GPS/MET  $N_e$  profiling based on close-up RO observations. The retrieved Abel-inversion  $N_e$  profiles at nearby occultation can provide horizontal but two-dimensional gradients using interpolation from a cubic spline fit and onto the LEO orbital plane. It was also shown that more aggregated occultation observations within a specified footprint can be used to retrieve more accurate  $f_oF2$  values. Tsai et al. (2011) presented a further RO  $N_e$  retrieval improvement to consider the effect of three-dimensional (3D) horizontal gradients using a phenomenological  $N_e$  model, namely the TaiWan Ionosphere Model (TWIM) Tsai et al. (2009). To improve the TWIM into a real-time model we also developed a time series autoregressive model to forecast short-term TWIM coefficients (Tsai et al. 2014a). In this research we carry out a feasibility study on ionospheric  $N_e$  profiling and 3D modeling in future FS7/COSMIC2. In the following Sect. 2 we illustrate the FS7/COSMIC2 simulation experiments using the TWIM and another independent ionospheric model (the NeQuick model) as backgrounds separately. In Sect. 3 we overview and evaluate  $N_e$  profiles, and retrieve  $f_oF2$  and  $hmF2$  values from the standard Abel-inversion method and also 3D  $N_e$  TWIM-construction models through two independent background simulations. In Sect. 4 an improved compensatory Abel-inversion scheme applied to FS7/COSMIC2 simulation data is illustrated and examined. We draw our discussions and summaries separately in Sects. 5 and 6.

## 2 COSMIC follow-on simulation experiments on ionospheric RO observations

The planned FS7/COSMIC2 mission will launch six satellites with 24° inclination at ~550-km altitude in 2016 and another six satellites with 72° inclination at ~750-km altitude in 2018 (Schreiner et al. 2012; <http://www.nspo.narl.org.tw>). In this study we used the Satellite Tool Kit (Version 10.0) to generate GPS (32 satellites), GLONASS (27 satellites), Galileo (4 satellites), and FS7/COSMIC2 (12 satellites) 1-Hz orbit data from the 1st to 100th day of year (DOY) in 2013 and then simulated Tri-G GNSS RO observations. Figure 1 shows 12 FS3/COSMIC2 LEO satellite orbits (in lines) and simulated GNSS RO observation locations (in dots) at peak  $N_e$  in 1-h duration. Each color represents one LEO satellite. There are more than 18,000 simulated RO observations per day when the LEO satellites can receive all available GNSS satellite signals at all antenna viewing angles from the LEO orbital planes. Because of insufficient antenna field of view referring to FS3/COSMIC RO observations, we limited the simulated RO observations to a maximum absolute antenna viewing angle at 60° and obtained ~13,000 observations per day, i.e. ~540 observations per hour as the example shown in Fig. 1. We note that 1 h is windowing duration for collecting RO  $N_e$  profiles used for further  $N_e$  modeling. Generally, simulated FS7/COSMIC2 RO observations in 1-h duration have good global coverage excluding two 80° longitude by 45° latitude gaps in high latitude. The two RO observation gaps will move westward of around 15° longitude per hour.

For each simulated RO observation, limb-viewing path TECs are calculated by integrating  $N_e$  values from the corresponding GNSS to LEO satellites under a straight-line propagation assumption. Two independent empirical  $N_e$  models used separately in this study are the TWIM and NeQuick (Leitinger et al. 2002; Brunini et al. 2013), also referred to as “true” (or background) ionospheres. The TWIM was constructed from near-vertical  $N_e$  profiles retrieved from FS3/COSMIC RO measurements and worldwide ionosonde  $foF2$  and  $foE$  data (Tsai et al. 2009). The TWIM exhibits vertically fitted  $\alpha$ -Chapman-type layers with distinct F2, F1, E, and D layers and surface spherical harmonic approaches for the fitted layer parameters including peak density, peak density height, and scale height. TWIM Chapman-layer parameter maps and associated data are available at “<http://isl.csr.ncu.edu.tw/>” hosted by the Center for Space and Remote Sensing Research, National Central University, Taiwan. To present 3D TWIM  $N_e$  results, Fig. 2a shows six latitude versus altitude  $N_e$  maps at 180°W, 120°W, 60°W, 0°E, 60°E, and 120°E longitudes and three latitude versus longitude  $N_e$  maps at 100, 300, and 500 km altitudes at 12 universal time (UT) of the 15th DOY in 2013. The NeQuick was developed by Leitinger et al. (2002) presenting ionospheric  $N_e$  by Epstein functions based on the CCIR ionospheric characteristics model. In this study the NeQuick model source code was provided by Ionospheric Radio Propagation Unit of the T/ICT4D Laboratory at [http://www.itu.int/dms\\_pub/itu-r/oth/04/R0A04000180001ZIPE.zip](http://www.itu.int/dms_pub/itu-r/oth/04/R0A04000180001ZIPE.zip). Figure 2b shows another global 3D  $N_e$  example of simulated “true” ionosphere from

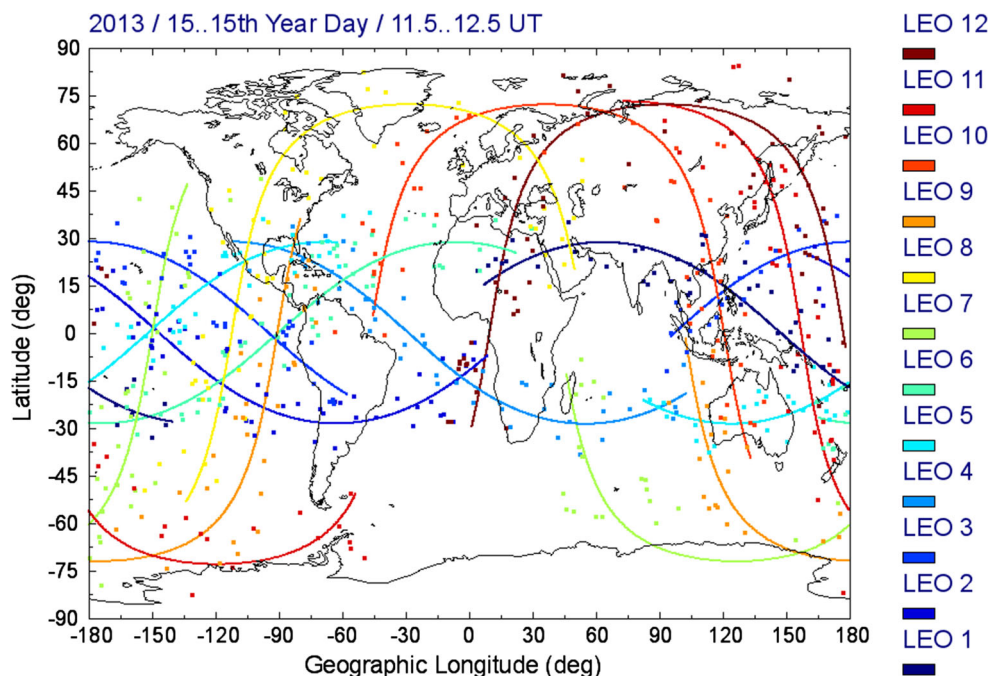


**Fig. 1** Simulated FS7/COSMIC2 LEO orbits and GNSS RO observation locations at peak  $N_e$  in 1-h duration are shown in lines and square dots separately. Each color represents one of twelve LEO satellites at 24° or 72° inclination angle

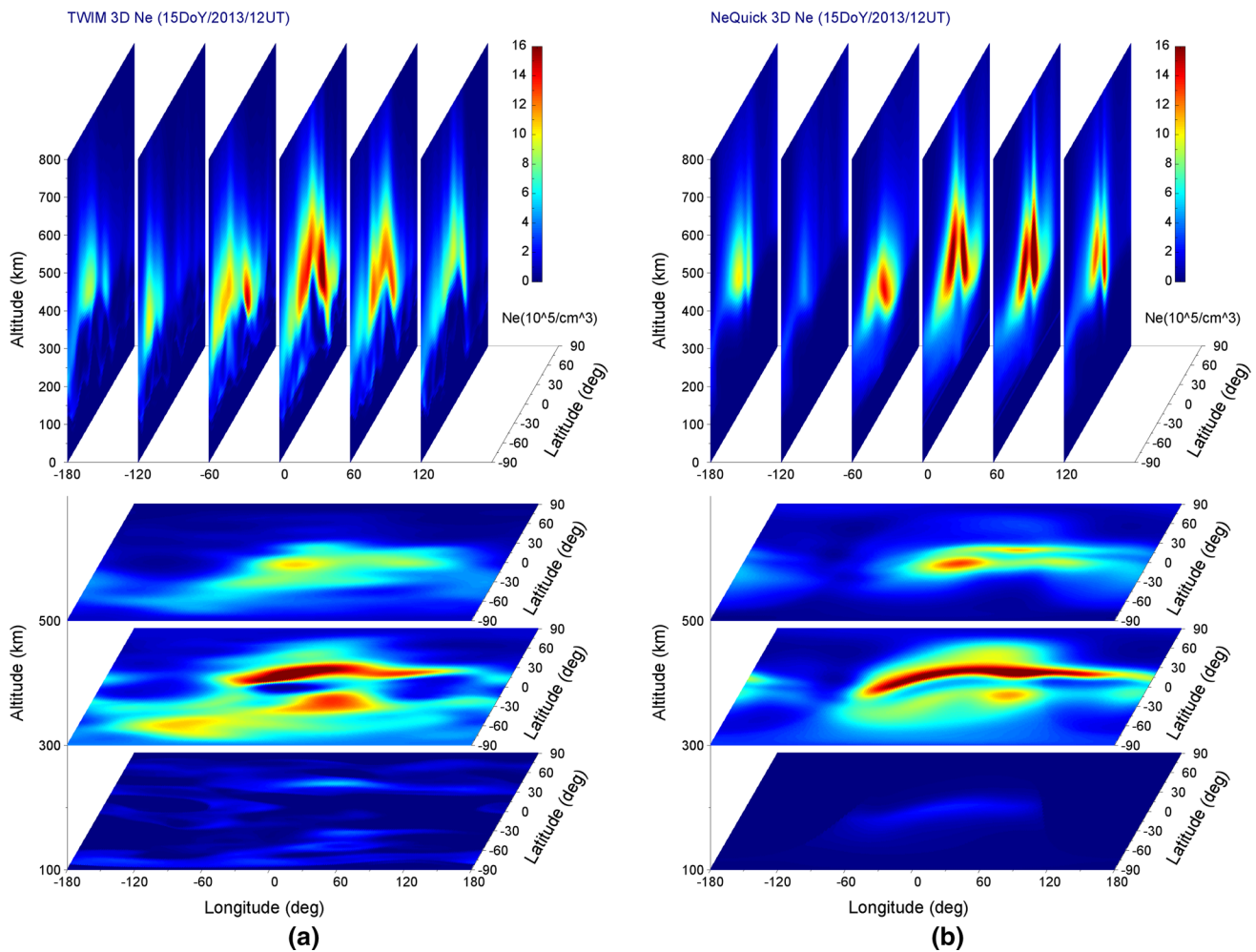


**Fig. 2** Two global 3D  $N_e$  examples are in respect to the *left (a)* and *right (b)* panels separately for simulated “true” background ionosphere from the TWIM and the NeQuick at 12 UT of the 15th DOY in 2013. The *upper images* show latitude versus altitude  $N_e$  variations at dif-

ferent longitudes ( $180^\circ\text{W}$ ,  $120^\circ\text{W}$ ,  $60^\circ\text{W}$ ,  $0^\circ\text{E}$ ,  $60^\circ\text{E}$ , and  $120^\circ\text{E}$ ); the *lower images* show latitude versus longitude  $N_e$  variations at different altitudes (100, 300, and 500 km)

the NeQuick using a F10.7 value of 135 at 12 UT of the 15th DOY in 2013. Both TWIM and NeQuick 3D  $N_e$  examples could show equatorial anomaly latitudinal distributions at different local times. To simulate limb-viewing TECs for FS7/COSMIC2 RO observations, a linear integration path resolution from 5 km (at 300-km altitude) to 35 km (at 0- or 600-km altitude) was used and can approach an accuracy of three orders less than 0.001 TECU which is the scientifically required TEC resolution in the FS3/COSMIC program.

### 3 COSMIC follow-on $N_e$ profiling and 3D $N_e$ modeling

GNSS occultation occurs when a GNSS satellite sets or rises behind the Earth’s ionosphere as seen by a LEO satellite. Each GNSS RO observation, therefore, consists of two sets of limb-viewing links with ray perigee ranging from the LEO

satellite altitude to the Earth’s surface at both the occulting and auxiliary sides. As described in the introduction,  $N_e$  profiles can be inverted using the Abel integral transform (Tricomi 1985) through calibrated TECs under assumptions including locally spherical symmetry on ionospheric  $N_e$ , straight-line ray propagation, static ionosphere, a known initial  $N_e$  at LEO orbit, and Earth’s spherical shape over the occultation duration. A spherical symmetry assumption on ionospheric  $N_e$  is used below the LEO altitude for the Abel inversion and also above the LEO altitude to determine the calibrated TEC (TEC’), which is derived by a limb-viewing TEC difference between the two limb-viewing GNSS-to-LEO TECs at the occulting side and its auxiliary side and with the same ray perigee range ( $r$ ). A  $N_e$  profile can thus be derived from top to bottom in altitude by applying the following integral equation to the calibrated TEC values:

$$N_e(r_t) = N_e(r_{LEO}) - \frac{1}{\pi} \int_{r_t}^{r_{LEO}} \frac{dTEC'(r)/dr}{\sqrt{r^2 - r_t^2}} dr, \quad (1)$$

where  $r_t$  is a tangent point radial distance of limb-viewing GNSS-to-LEO path, and  $N_e(r_{LEO})$  is a known initial  $N_e$  at the LEO altitude ( $r_{LEO}$ ). In this study, FS7/COSMIC2 RO observations were simulated by calculating the limb TEC values separately through independent TWIM and NeQuick models. Using both of the TWIM- and NeQuick-background simulation data (6141 GNSS RO observations) during the range of (11.5–12.5) UT from the 5th to 15th

DOY in 2013,  $N_e$  profiles can be retrieved by applying the standard Abel-inversion method as shown in Eq. (1), and the corresponding  $foF_2$  and  $hmF_2$  values can be obtained at peak  $N_e$  by inspection. Figure 3a shows a scatter plot of the resulting retrieved  $foF_2$  (referred to the left y-axis) versus “true”  $foF_2$  from the background TWIM (referred to the x-axis) and also their corresponding mean (in red) and RMS (in green)  $foF_2$  difference profiles (referred to the right y-axis) at a 0.1 MHz step as a function of “true” TWIM  $foF_2$ . Using the same TWIM-background simula-

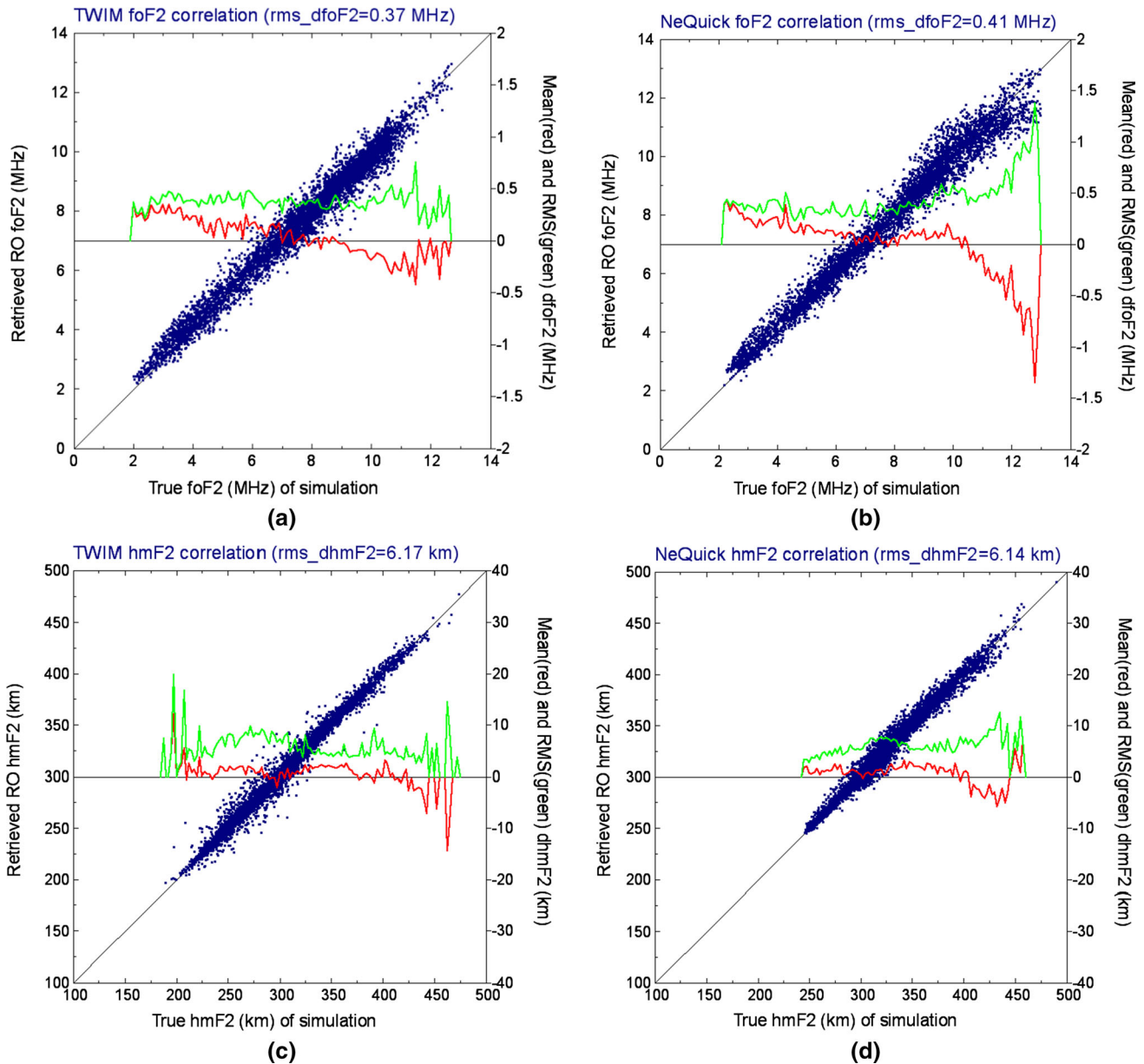


**Fig. 3** Scatter plots of retrieved  $foF_2$  ( $hmF_2$ ) versus “true”  $foF_2$  ( $hmF_2$ ) are shown in the left-upper and right-upper (left-lower and right-lower) images separately based on the TWIM- and NeQuick-background simulation data and using the standard Abel inversion

method. The images also show their corresponding mean (in red) and root-mean-square (RMS, in green)  $foF_2$  or  $hmF_2$  difference profiles (referred to the right y-axis) as a function of “true” background  $foF_2$  or  $hmF_2$

tion data, Fig. 3c shows a scatter plot of the retrieved  $hmF_2$  versus “true”  $hmF_2$  from the background TWIM and also their corresponding mean (in red) and RMS (in green)  $hmF_2$  difference profiles at a 1 km step. As shown in Fig. 3a, c, and b, d show the retrieval  $foF_2$  and  $hmF_2$  results but applied to the NeQuick-background simulation data during the range of (11.5–12.5) UT from the 5th to 15th DOY in 2013. The retrieved  $foF_2$  and  $hmF_2$  results on the other simulation days were obtained in a similar manner as shown in Fig. 3 and are not shown in this paper. Applying both TWIM- and NeQuick-ground simulation data, the averaged RMS retrieval errors on  $foF_2$  and  $hmF_2$  are less than 0.41 MHz and 6.2 km, respectively, and the standard Abel inversion generally provides good retrieved results for  $foF_2$  and  $hmF_2$ , which are the most important ionospheric characteristic parameters. As seen from Fig. 3a, b, the retrieved  $foF_2$  values are biased high, i.e. overestimated, with respect to “true”  $foF_2$  from both the background TWIM and NeQuick with a maximum 0.4 MHz mean difference between 2 and 4 MHz of  $foF_2$ . However, such positive biases are decreased when the  $foF_2$  values increase. The absolute mean errors are  $<0.1$  MHz in general when the  $foF_2$  values are between 6 and 10 MHz. On the other high  $foF_2$  side retrieved  $foF_2$  values are biased low (underestimated) with respect to the “true” background values when  $foF_2$ s are larger than 10 MHz. The underestimated condition can be approached to a maximum mean difference  $\sim 1$  MHz for  $foF_2$  values larger than 12 MHz. In practice, retrieval errors on  $N_e$  could be accumulated from top to bottom during a standard Abel inversion. Horizontal inhomogeneous  $N_e$  for a given occultation is believed to be the main source of error. Either overestimated or underestimated conditions can be typically explained by ionospheric electron densities that are distributed under even symmetry as a valley or crest within a targeted occultation area and with limb-viewing GNSS-to-LEO tangent points at a locally minimum or maximum, respectively. The observed valley (crest) would be spread out after the Abel inversion and the retrieved  $N_e$  (or  $foF_2$ ) values at the tangent points are thus overestimated (underestimated) to the true values. As seen from Figs. 3c and 3d the retrieved  $hmF_2$  values are biased high lightly ( $<2$  km) with respect to both “true” TWIM- and NeQuick-background values when  $hmF_2$  values are less than 400 km. Except for some sparse results, retrieved  $hmF_2$ s are biased low (underestimated) with respect to both TWIM- and NeQuick-background values when  $hmF_2$ s are larger than 400 km. We note that using the standard Abel inversion, retrieved  $hmF_2$  values have better results than retrieved  $foF_2$ s in total.

Accurate and precise real-time ionosphere modeling is important to radio sky-wave communications, satellite positioning, and remote sensing. In our earlier investigations, Tsai et al. (2009) developed the TWIM which consists of

fitted  $\alpha$ -Chapman-type layers, shown as the following equation representing 3D  $N_e$  in latitude ( $\theta$ ), longitude ( $\lambda$ ), and altitude ( $h$ ).

$$N_e(\theta, \lambda, h) = \sum_{i=1}^4 N_m^i(\theta, \lambda) \cdot e^{\frac{1}{2} \left[ 1 - \frac{h-h_m^i(\theta, \lambda)}{H^i(\theta, \lambda)} - e^{-\frac{h-h_m^i(\theta, \lambda)}{H^i(\theta, \lambda)}} \right]}, \quad (2)$$

where each  $i$  means a physical F2, F1, E, or D layer according to height and ion distribution from top to bottom. Each layer is generally characterized by an  $\alpha$ -Chapman-type function described by peak  $N_e$  ( $N_m$ ), peak density height ( $h_m$ ), and scale height ( $H$ ) parameters. Each Chapman-layer parameter is presented as a following  $\Gamma()$  function in latitude and longitude and constructed using spherical harmonic analysis (Davis 1989) with specified local or universal time at a half-hour temporal resolution of

$$\Gamma(\theta, \lambda) = \sum_{m=0}^3 \sum_{n=0}^{q_m} [A_{nm} U_{nm}(\theta, \lambda) + B_{nm} V_{nm}(\theta, \lambda)], \quad (3a)$$

where

$$U_{nm}(\theta, \lambda) = \sqrt{\frac{2n+1}{2\pi} \frac{(n-m)!}{(n+m)!}} P_{nm}(\cos \theta) \cos m\lambda, \quad (3b)$$

and

$$V_{nm}(\theta, \lambda) = \sqrt{\frac{2n+1}{2\pi} \frac{(n-m)!}{(n+m)!}} P_{nm}(\cos \theta) \sin m\lambda \quad (n = 0, 1, 2, \dots, q_m; m = 0, 1, 2, \text{ or } 3), \quad (3c)$$

and  $P_{nm}()$  is the familiar associated Legendre polynomial of the first kind of degree  $n$  and order  $m$ . In our earlier investigations (Tsai et al. 2009), the TWIM coefficients ( $A_{nm}$  and  $B_{nm}$ ) of Chapman-layer parameters can be determined using the least squares method at a specified  $m$ -order and  $n$ -degree spherical harmonics analysis, and an optimization analysis on order and degree numbers has been implemented by truncating the high spectrum harmonics based on a least-square fitting. The optimum cut-offs used in this study are a maximum order of 3 and a maximum degree of 20 for each order. For other details concerning the TWIM performance and evaluation, interested readers can refer to Tsai et al. (2014b) and Macalalad et al. (2012, 2014). Note that in order to ensure good global and dense data coverage, every half-hour TWIM coefficients ( $A_{nm}$  and  $B_{nm}$ ) were estimated using a 1-h (in UT) and 30-day window on retrieved FS3/COSMIC  $N_e$  profiles where more Gaussian-shaped weight was credited to the profile closer to the day of interest. In this simulation study we obtained more than an order of magnitude in the number of RO  $N_e$  profiles, and a windowing day number to collect  $N_e$  profiles and derive every half-hour FS7/COSMIC2

TWIM coefficient set could be much less. After trying from 1 to 9 days on windowing retrieved FS7/COSMIC2  $N_e$  profiles to produce 3D  $N_e$  models (also under a TWIM construction), we obtained a minimum RMS  $N_e$  error when a 3-day or 9-day window was used at the TWIM- or NeQuick-background simulation experiment. Additional discussions will be continued in Sect. 5. The resulting 3D  $N_e$  models are similar to the background TWIM or NeQuick as shown in Fig. 2. Figure 4a, b shows six latitude versus altitude modeled  $N_e$  error maps at 180°W, 120°W, 60°W, 0°E, 60°E, and 120°E longitudes and three latitude versus longitude  $N_e$  error maps at 100, 300, and 500 km altitudes at 12 UT on the 15th DOY in 2013. The modeling results using TWIM-background simulation data are slightly better than those using NeQuick-background simulation data. This can be explained by that a background TWIM for simulation and its resulting modeled TWIM have a same kind of 3D  $N_e$  construction.

### 4 Compensatory Abel-inversion $N_e$ retrieval and improved 3D $N_e$ model

The true ionospheric  $N_e$  as both background TWIM and NeQuick used in this simulation study is never spherically symmetric. To retrieve more precise RO  $N_e$  profiles calibrated TECs should not be used directly and inverted using the Abel integral transform as shown in Eq. (1). This process could be compensated using limb-viewing path TEC differences from a spherically symmetric ionosphere. As shown in the following Eq. (4), such path TEC differences for compensating could be calculated by integrating limb-viewing  $N_e$  differences between the true  $N_e(r, \theta, \lambda)$  and its spherically symmetric model where  $N_e(r, \theta_t(r), \lambda_t(r))$  values represent the true  $N_e$  values at a set of limb-viewing tangent points with different ray perigee range  $r$  during a RO observation.

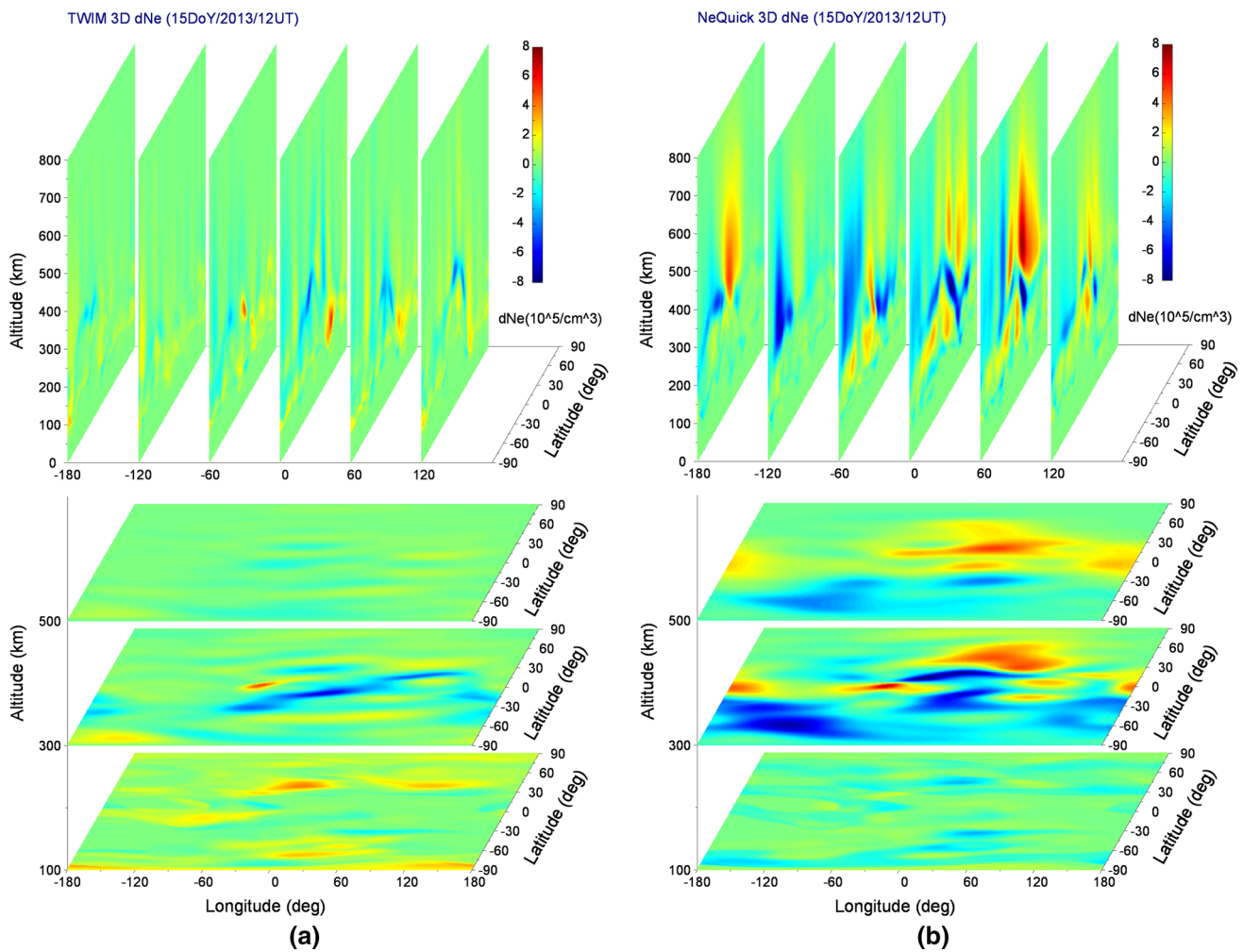


**Fig. 4** Two resulting modeled 3D  $N_e$  differences, i.e. errors, are in respect to the *left (a)* and *right (b)* panels separately from “true” TWIM- and NeQuick-background ionospheres at 12 UT of the 15th DOY in 2013. The *upper images* show latitude versus altitude  $N_e$  difference

variations at different longitudes (180°W, 120°W, 60°W, 0°E, 60°E, and 120°E); the *lower images* show latitude versus longitude  $N_e$  difference variations at different altitudes (100, 300, and 500 km)

The Abel inversion process can then be applied to such compensated path TECs ( $\text{TEC}^*$ ) as following and improve  $N_e$  profiling:

$$\text{TEC}^*(r) = \text{TEC}'(r) + \int_{P_1}^{P_2} (N_e(r, \theta_t(r), \lambda_t(r)) - N_e(r, \theta, \lambda)) dl, \quad \text{and} \quad (4)$$

$$N_e^*(r_t) = N_e(r_{\text{LEO}}) - \frac{1}{\pi} \int_{r_t}^{r_{\text{LEO}}} \frac{d\text{TEC}^*(r)/dr}{\sqrt{r^2 - r_t^2}} dr, \quad (5)$$

where  $P_2$  is the corresponding calibration position of a LEO occultation position  $P_1$  having the same radial distance along GNSS-to-LEO line-of-sight. However, the true ionospheric  $N_e$  is never known. When calculating compensated TECs using Eq. (4) it becomes necessary to assume a 3D ionospheric  $N_e$ , and a more realistic ionospheric model could be used to retrieve more precise  $N_e$  profiles and vice versa. In this simulation study two independent ionospheric models, the TWIM and NeQuick, were used separately as background ionospheres to simulate limb-viewing GNSS-to-LEO TEC values. Near vertical  $N_e$  profiles were retrieved first as initial profiles by applying the standard Abel inversion method on calibrated TECs. After fitting  $\alpha$ -Chapman-type multi-layer to the retrieved  $N_e$  profiles and then using surface spherical harmonics for the derived layer parameters, we obtained two different TWIM-construction models separately using TWIM- and NeQuick-background simulation data. These derived TWIM-construction models could then be used as an assumed ionosphere to determine the compensated limb-viewing TECs using Eq. (4) for the next-iteration  $N_e$  profiles followed with TWIM-construction models again. To clarify more details of the compensatory Abel inversion scheme applied to FS7/COSMIC2 simulation data and even future real observations, the main process steps are listed as follows:

1. Simulate (or determine) 1-Hz limb-viewing GNSS-to-LEO TECs at both occulting and auxiliary sides by integrating  $N_e$  through a background model (or using dual-frequency excess phases from real observations).
2. Interpolate simulated (or real measured) ionospheric delays at evenly spaced radial distances and determine calibrated TEC to be a TEC difference between two limb-viewing GNSS-to-LEO TECs at an occulting side and its auxiliary side and with a same ray perigee range.
3. Apply the standard Abel inversion method to a set of calibrated TECs with evenly spaced radial distances and retrieve initial ionospheric  $N_e$  profiles.
4. Fit each retrieved  $N_e$  profile into  $\alpha$ -Chapman-type multi-layer using the least squares method. Each two-dimensional global Chapman-layer parameter map can

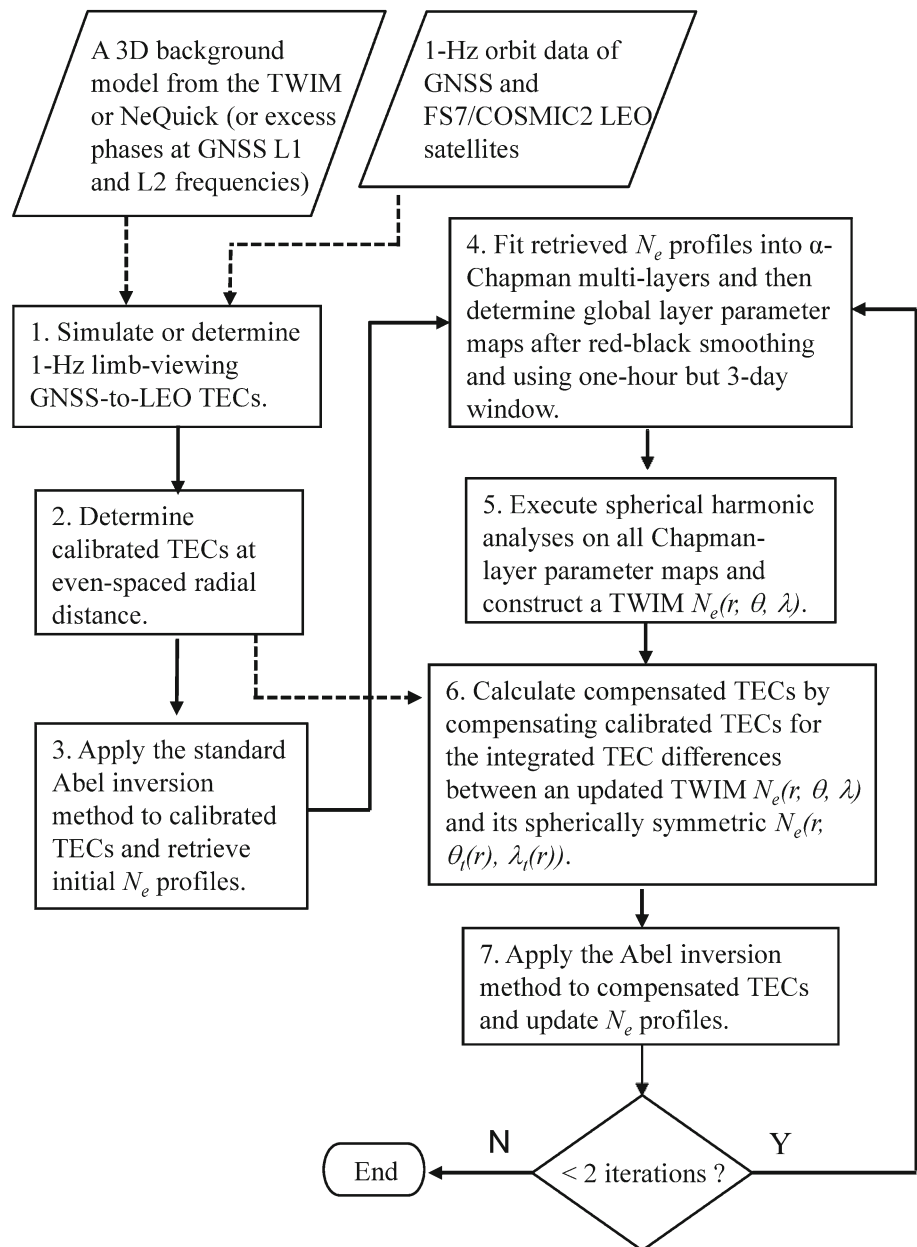
then be obtained after red-black smoothing (Press et al. 1992) with a pixel resolution of  $2^\circ$  in latitude and  $4^\circ$  in longitude and at a 1-h (in UT) but 3-day window on retrieved  $N_e$  profiles (and 1-day ionosonde  $foF2$  and  $foE$  data set for real observations).

5. Execute spherical harmonic analyses on all Chapman-layer parameter maps and construct a TWIM  $N_e(r, \theta, \lambda)$ .
6. Calculate compensated path TECs by compensating calibrated TECs [from Step (2)] for the integrated limb-viewing TEC differences between the previous updated TWIM  $N_e(r, \theta, \lambda)$  and its spherically symmetric  $N_e(r, \theta_t(r), \lambda_t(r))$  as given in Eq. (4).
7. Apply the Abel inversion method again to the previous updated compensated TECs and retrieve the next-iteration  $N_e$  profiles.
8. Repeat Steps (4), (5), (6), and (7) to approach stable  $N_e$  profiles and 3D  $N_e$  model.

The associated flowchart is also summarized and shown in Fig. 5. Note that after our earlier investigations (Tsai et al. 2009, 2011), we further improved the  $\alpha$ -Chapman-type multi-layer fitting to have different coordinates at different layers because retrieved RO  $N_e$  profiles are not really vertical. In addition, to have complete worldwide coverage and obtain more precise 3D  $N_e$  models, we included more retrieved  $N_e$  profiles from previous days (and during 1-h UT window) and also executed red-black smoothing on empty pixels on every Chapman-layer parameter map, making interlaced passes of updating the “red” pixels (like the red squares of a checkerboard) and then updating the “black” pixels (like the black squares). The retrieved  $foF2$ s and  $hmF2$ s evaluations through the compensatory Abel-inversion scheme (after two iterations) on the FS7/COSMIC2 TWIM-background (NeQuick-background) simulation experiment are shown in Fig. 6. Comparing Fig. 6a, b with Fig. 3a, b separately, the overestimates (underestimates) at low (high) retrieved  $foF2$ s, are improved to give better agreements with both background ionospheric models. The average  $\text{RMS}foF2$  differences are significantly improved from 0.37 (0.41) MHz to 0.22 (0.29) MHz after one iteration and then 0.20 (0.28) MHz after two iterations based on the TWIM-background (NeQuick-background) simulation data, i.e. the two-iteration improvement is 46% (32%) in relative percentage. Comparing Fig. 6c, d with Fig. 3c, d separately, the slight overestimates (underestimates) at low (high) retrieved  $hmF2$ s are also improved. The average  $\text{RMS}hmF2$  differences are improved from 6.17 (6.14) km to 4.85 (5.89) MHz after one iteration and then 4.78 (5.86) MHz after two iterations based on the TWIM-background (NeQuick-background) simulation data, i.e. the two-iteration improvement is 21% (4.6%) in relative percentage. The retrieved  $foF2$  and  $hmF2$  results were obtained in a similar manner after two iterations of the



**Fig. 5** A flowchart of the compensatory Abel inversion scheme applied to FS7/COSMIC2 simulation data (or future real observations)



compensatory Abel-inversion scheme and are not discussed and shown in this paper.

### 5 Discussions on COSMIC follow-on feasibility study

As discussed in Sect. 2 the planned FS7/COSMIC2 mission will have about 13,000 RO observations per day when the twelve LEO satellites can receive all available GNSS satellite signals and at a maximum antenna viewing angle of 60° from the LEO orbital planes. There are approximately 10 times more RO observations than FS3/COSMIC, but it is still not enough to cover worldwide and complete 3D  $N_e$  models. It becomes necessary to include more

retrieved  $N_e$  profiles from previous days for  $N_e$  modeling. As shown in Fig. 7 a dotted blue (or gray) line represents RMS modeled  $N_e$  errors versus the windowing day number for 1st-iteration (or 2nd-iteration) FS7/COSMIC2 simulations using a TWIM-background ionosphere, a dotted red (or yellow) line for 1st-iteration (or 2nd-iteration) FS7/COSMIC2 simulations using a NeQuick-background, and a dotted green line for 1st-iteration FS3/COSMIC simulations using a TWIM-background ionosphere. Note that using a same windowing day number there are more or less one-order larger  $N_e$  errors in the FS3/COSMIC simulation results compared to both the TWIM-background and NeQuick-background FS7/COSMIC2 simulations. This means more and denser

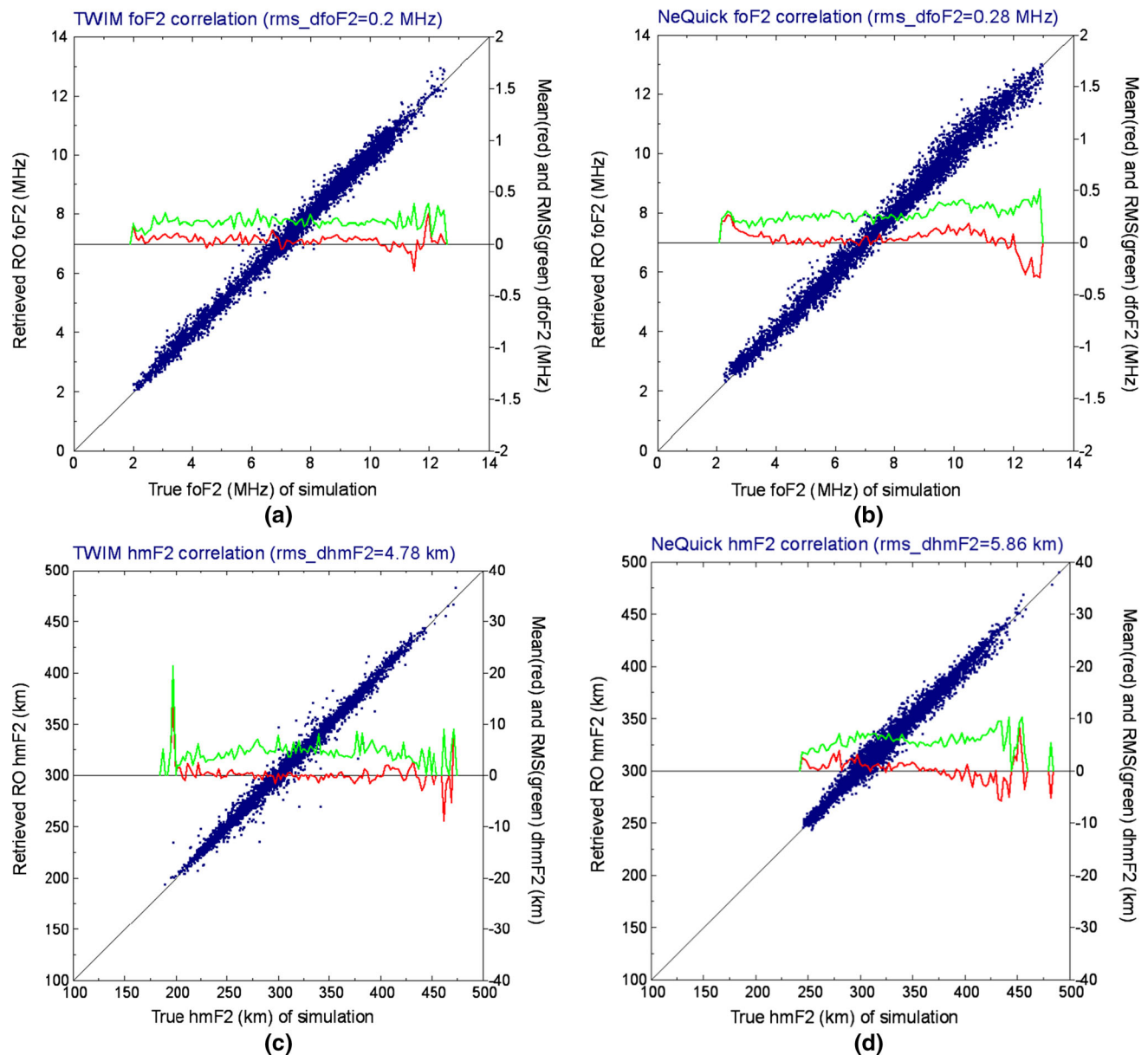


**Fig. 6** As in Fig. 3 but after two iterations of the compensatory Abel inversion scheme

observations produce better modeling results. When the windowing day numbers are increased, the RMS  $N_e$  errors are decreased because more observations are included, and the RMS  $N_e$  errors reach a minimum at a windowing day number of 3 or 26 separately in respect to FS3/COSMIC or FS7/COSMIC2 simulation experiments using a TWIM-background ionosphere. This can be realized that because the background TWIM varies daily,  $N_e$  modelling results could be out of focus when including more retrieved  $N_e$  profiles from previous days, and a minimum  $N_e$  error would be reached at a certain windowing day number. However, the NeQuick is a monthly 3D  $N_e$  model using F10.7 radio flux or R12 sunspot number as the input. For FS7/COSMIC2

simulation experiments in the same month and F10.7 radio flux, the NeQuick backgrounds are the same and the resulting  $N_e$  errors are decreased and then saturated when the windowing day numbers are increased and thus more  $N_e$  profiles are included. Finally, as shown in Fig. 7, the TWIM-background FS7/COSMIC2 simulations have better modeling results (the dotted blue and grey lines) than the NeQuick-background simulations (the dotted red and yellow lines). Two-iteration modeled  $N_e$  results are more improved than one-iteration results in TWIM-background FS7/COSMIC2 simulations but not significant in NeQuick-background FS7/COSMIC2 simulations. This could be explained using the same 3D  $N_e$

construction on a modeled TWIM and a background TWIM but not on a background NeQuick.

The standard Abel-inversion method can retrieve RO  $N_e$  profiles from the top to the bottom of a RO observation based on a spherical symmetry assumption. It is possible that  $N_e$  errors are accumulated and getting larger when a profile is retrieved downward. Based on the same FS7/COSMIC2

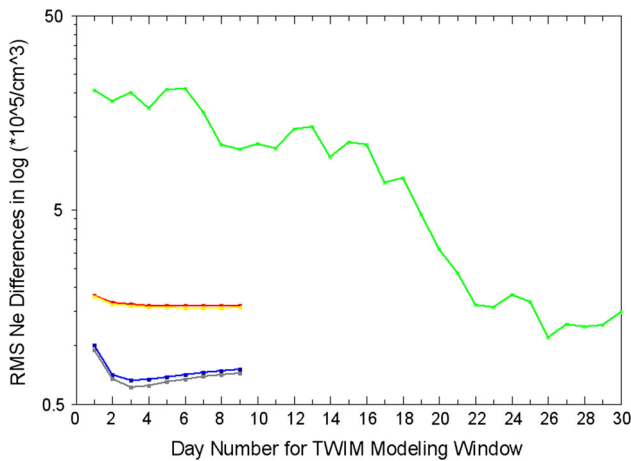
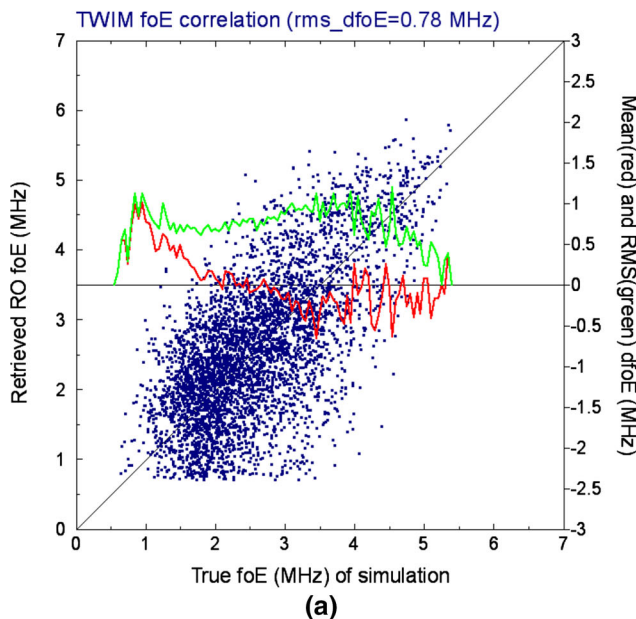


**Fig. 7** RMS modeled  $N_e$  errors versus windowing day number: a dotted blue (or grey) line for 1st-iteration (or 2nd-iteration) FS7/COSMIC2 simulations using a TWIM-background ionosphere, a dotted red (or yellow) line for 1st-iteration (or 2nd-iteration) FS7/COSMIC2 simulations using a NeQuick-background, and a dotted green line for 1st-iteration FS3/COSMIC2 simulations using a TWIM-background ionosphere



TWIM-background simulation data used in the previous studies, Fig. 8a, b shows scatter plots of the retrieved  $foE$  versus “true” background  $foE$  and also their mean and RMS  $foE$  difference profiles using the standard Abel inversion method and the two-iteration compensatory Abel inversion scheme, respectively. As seen from Fig. 8a, the retrieved  $foE$  values are also overestimated ( $<1$  MHz) when  $foE$  values are less than 2.5 MHz, and retrieved  $foE$ s are underestimated usually at the other high  $foE$  side. This could mean that a  $N_e$  profile with high  $foF2$  has high  $foE$  in usual and overestimated (underestimated)  $N_e$  errors at low (high)  $foF2$ s could be accumulated downward to produce overestimated (underestimated)  $foE$ s. After making the comparison between Fig. 8a, b, the overestimates (underestimates) located at low (high)  $foE$  are improved and give better agreement with the “true” TWIM background. The average RMS  $foE$  differences are also improved from 0.78 to 0.66 MHz after one iteration and then 0.62 MHz after two iterations of compensatory Abel inversion scheme, i.e. the two-iteration improvement is 21% in relative percentage. In summary, retrieval  $foE$ s have larger errors than retrieved  $foF2$ s from the simulation experiment, and the  $foE$  retrieval using the compensatory Abel-inversion scheme is still improved but less than the  $foF2$  retrieval improvement. It is difficult to obtain “true” NeQuick-background  $foE$ , and thus a  $foE$  retrieval examination was not completed in these NeQuick-background simulations.

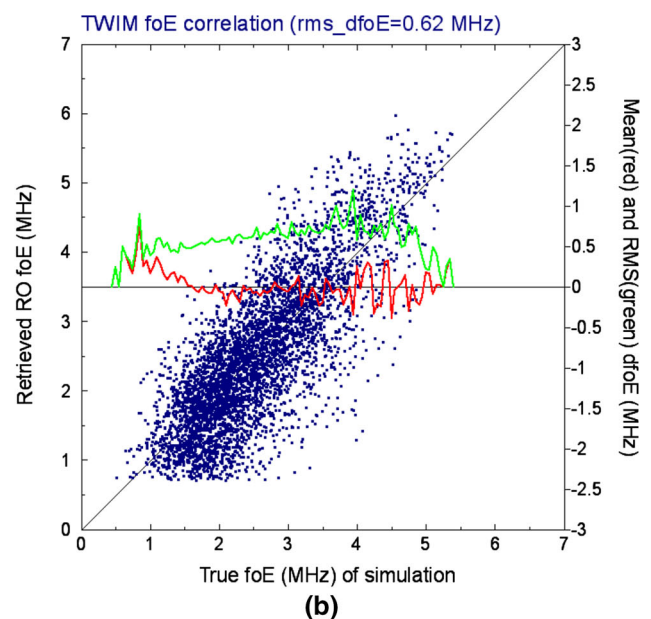


**Fig. 8** Based on FS7/COSMIC2 TWIM-background simulations, scatter plots of retrieved  $foE$  versus “true”  $foE$  are shown in the left (a) and right (b) images using the standard Abel inversion method and the two-iteration compensatory Abel inversion scheme, respectively. The

images also show their corresponding mean (in red) and root-mean-square (RMS, in green)  $foE$  difference profiles (referred to the right y-axis) as a function of “true” background  $foE$

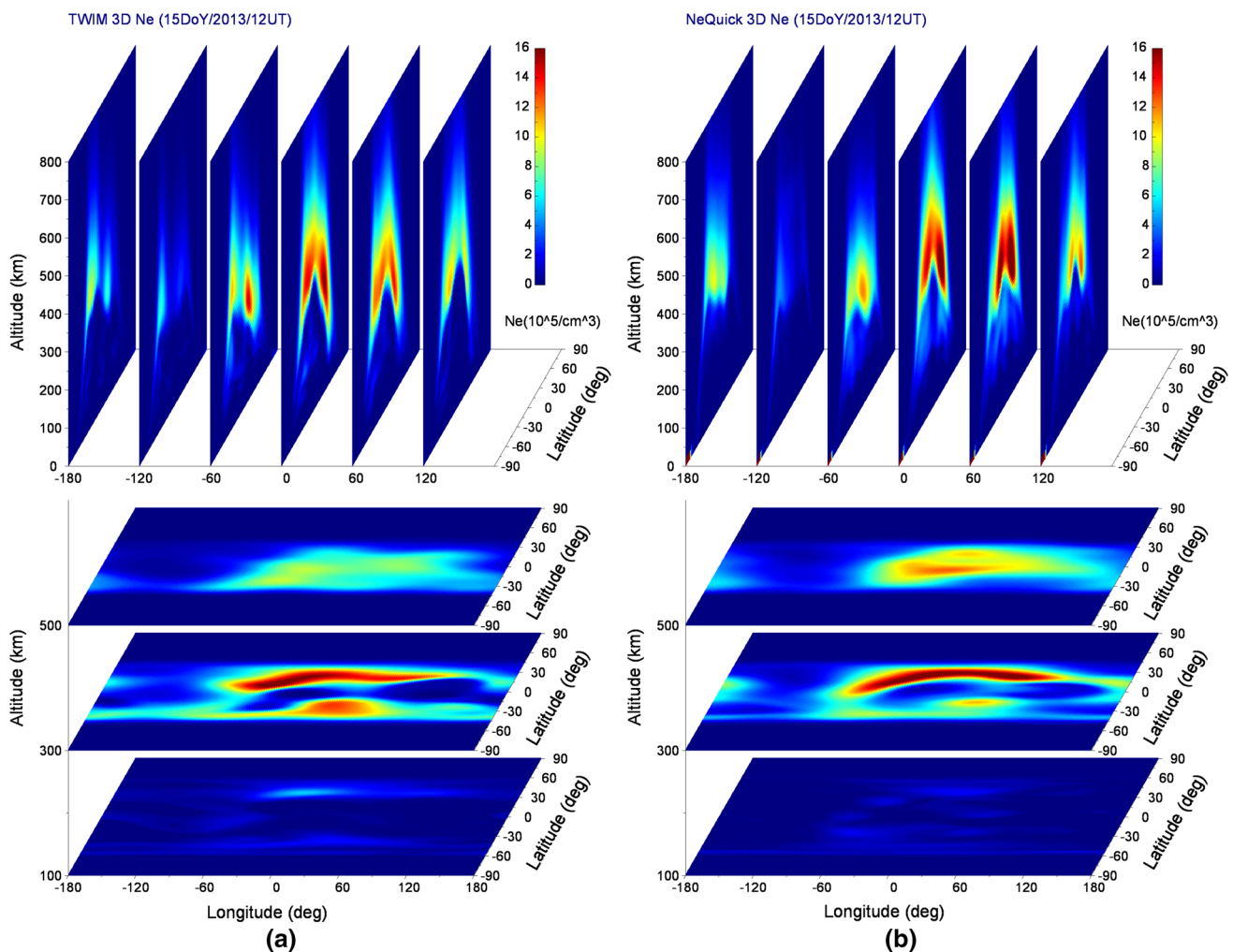


**Fig. 9** As in Fig. 2 two resulting 3D  $N_e$  models shown in the left (a) panel from TWIM-background simulations and in the right (b) panel from NeQuick-background simulation and based on the simulated RO observations from only six  $24^\circ$ -inclination LEO satellites

As described the planned FS7/CISMIC2 mission will launch the first six satellites with  $24^\circ$  inclination in 2016 and another six satellites with  $72^\circ$  inclination in 2018. To illustrate the different effects of using only six low ( $24^\circ$ ) inclination LEO satellite constellations in modeling the ionosphere, we show both resulting TWIM-simulation and NeQuick-simulation 3D  $N_e$  models in Fig. 9 using the simulated RO observations from only six  $24^\circ$ -inclination LEO satellites and two iterations on the compensatory Abel inversion scheme. In our studies a 6-day window was used to collect  $N_e$  profiles and obtain a minimum RMS  $N_e$  error on the TWIM-background simulations. This is expected because only six LEO satellites were used. In the  $<40^\circ$  latitude regions the resulting  $N_e$  models are as good as those using all twelve LEO satellites at both low- and high-inclination orbits. However, in the  $>40^\circ$  latitude regions the modeled  $N_e$  values are not reliable.

## 6 Conclusions

This paper presents a FS7/COSMIC2 feasibility study using a compensatory Abel inversion scheme on  $N_e$  profiling and 3D modelling through two independent TWIM- and NeQuick-background simulation experiments. It is expected that  $>500$  RO  $N_e$  profiles can be obtained per hour in the future FS7/COSMIC2 program through twelve LEO satellites to receive Tri-G (GPS, GLONASS and Galileo) beacon signals. To collect enough  $N_e$  profiles for obtaining a precise 3D  $N_e$  model, only a 3-day window for future FS7/COSMIC2 program is needed and is 10 times shorter than a 30-day window used in FS3/COSMIC. Based on the compensatory Abel-inversion scheme, the derived TWIM-construction model could be used as an assumed ionosphere to determine compensated limb-viewing TECs for the next-iteration  $N_e$  profiles and then TWIM-construction models

again. The simulation results show that the improvements in RMS retrieved *foF2*, *hmF2*, and *foE* differences are 46 % (32 %), 21 % (4.6 %), and 21 %, respectively, in relative percentage over the standard Abel inversion at the TWIM-background (NeQuick-background) simulation experiment. The RMS modeling errors are about one order less than those from the FS3/COSMIC simulations.

**Acknowledgments** This work has been supported by Ministry of Science and Technology, Taiwan, R.O.C. through Project Nos. MOST 103-2111-M-008-022 and NSC 102-2923-M008-002-MY3. The authors express their appreciation to Ionosphere Radio Propagation Unit of the T/ICT4D Laboratory for providing the NeQuick model source code. The authors would also like to thank UCAR's CDAAC and NSPO Satellite Operations Control Center (SOCC) for providing FS3/COSMIC satellite data.

## References

- Aragon-Angel A, Hernandez-Pajares M, Juan JM, Sanz J (2009) Obtaining more accurate electron density profiles from bending angle with GPS occultation data: FORMOSAT-3/COSMIC constellation. *Adv Space Res* 43:1694–1701. doi:[10.1016/j.asr.2008.10.034](https://doi.org/10.1016/j.asr.2008.10.034)
- Aragon-Angel A, Hernandez-Pajares M, Zornoza MJ, Subirana JS (2010) Improving the Abel transform inversion using bending angles from FORMOSAT-3/COSMIC. *GPS Solut* 14:23–33. doi:[10.1007/s10291-009-0147-y](https://doi.org/10.1007/s10291-009-0147-y)
- Borsche M, Kirchengast G, Foelsche U (2007) Tropical tropopause climatology as observed with radio occultation measurements from CHAMP compared to ECMWF and NCEP analyses. *Geophys Res Lett* 34:L03702. doi:[10.1029/2006GL027918](https://doi.org/10.1029/2006GL027918)
- Brunini C, Azpilicueta Francisco, Nava Bruno (2013) A technique for routinely updating the ITU-R database using radio occultation electron density profiles. *J Geodesy*. doi:[10.1007/s00190-013-0648-x](https://doi.org/10.1007/s00190-013-0648-x)
- Cucurull L, Derber JC, Treadon R, Purser RJ (2007) Assimilation of global positioning system radio occultation observations into NCEP's global data assimilation system. *Mon Weather Rev* 135:3174–3193. doi:[10.1175/MWR3461.1](https://doi.org/10.1175/MWR3461.1)
- Davis HF (1989) *Fourier series and orthogonal functions*. ISBN-13:978-0486659732. Dover Publications Inc, New York
- Fjeldbo G, Eshleman VR (1969) Atmosphere of Venus as studied with the Mariner V dual radio frequency occultation experiment. *Radio Sci* 4:879–897. doi:[10.1029/RS004i010p00879](https://doi.org/10.1029/RS004i010p00879)
- Hajj GA, Romans LJ (1998) Ionospheric electron density profiles obtained with the Global Positioning System: results from the GPS/MET experiment. *Radio Sci* 33(1):175–190. doi:[10.1029/97RS03183](https://doi.org/10.1029/97RS03183)
- Hajj GA, Lee LC, Pi X, Romans LJ, Schreiner WS, Straus PR, Wang C (2000) COSMIC GPS ionospheric sensing and space weather. *Terr Atmos Ocean Sci* 11(1):235–272
- Hernández-Pajares M, Juan JM, Sanz J (2000) Improving the Abel inversion by adding ground GPS data to LEO radio occultation in ionospheric sounding. *Geophys Res Lett* 27(16):2743–2746. doi:[10.1029/2000GL000032](https://doi.org/10.1029/2000GL000032)
- Kursinski ER, Hajj GA, Schofield JT, Linfield RP, Hardy KR (1997) Observing Earth's atmosphere with radio occultation measurements using the Global Positioning System. *J Geophys Res* 102:23429–23465. doi:[10.1029/97JD01569](https://doi.org/10.1029/97JD01569)
- Leitinger R, Radicella S, Nava B (2002) Electron density models for assessment studies—new developments. *Acta Geodet Geophys Hung* 37:183–193. doi:[10.1556/AGeod37.2002.2-3.7](https://doi.org/10.1556/AGeod37.2002.2-3.7)
- Leroy SS, Anderson JG, Dykema JA (2006) Testing climate models using GPS radio occultation: a sensitivity analysis. *J Geophys Res* 111:D17105. doi:[10.1029/2005JD006145](https://doi.org/10.1029/2005JD006145)
- Macalalad EP, Tsai L-C, Wu J, Liu CH (2012) Application of the TaiWan Ionospheric Model to single-frequency ionospheric delay corrections for GPS Positioning. *GPS Solut*. doi:[10.1007/s10291-012-0282-8](https://doi.org/10.1007/s10291-012-0282-8)
- Macalalad EP, Tsai L-C, Wu J (2014) Performance evaluation of different ionospheric models in single-frequency code-based differential GPS positioning. *GPS Solut*. doi:[10.1007/s10291-014-0422-4](https://doi.org/10.1007/s10291-014-0422-4)
- Pi X, Mannucci AJ, Iijima BA, Wilson BD, Komjathy A, Runge TF, Akopian V (2009) Assimilative modeling of ionospheric disturbances with FORMOSAT-3/COSMIC and ground-based GPS measurements. *Terr Atmos Ocean Sci* 20:273–285. doi:[10.3319/TAO.2008.01.04.01\(F3C\)](https://doi.org/10.3319/TAO.2008.01.04.01(F3C))
- Press WH, Teukolsky SA, Vetterling WT, Flannery BP (1992) *Numerical recipes in C: the art of scientific computing*, 2nd edn. ISBN 0-521-43108-5. Cambridge Univ. Press, New York
- Rocken C, Anthes R, Exner M, Hunt D, Sokolovskiy S, Ware R, Gorbunov M, Schreiner W, Feng D, Herman B, Kuo Y, Zou X (1997) Analysis and validation of GPS/MET data in the neutral atmosphere. *J Geophys Res* 102(D25):29849–29866. doi:[10.1029/97JD02400](https://doi.org/10.1029/97JD02400)
- Schreiner WS, Sokolovskiy SV, Rocken C, Hunt DC (1999) Analysis and validation of GPS/MET radio occultation data in the ionosphere. *Radio Sci* 34(4):949–966. doi:[10.1029/1999RS900034](https://doi.org/10.1029/1999RS900034)
- Schreiner WS, Yue X, Kuo Y-H, Mamula D, Ector D (2012) Satellite constellations for space weather and ionospheric studies: status of the COSMIC and planned COSMIC-2 missions. In: *Proceedings of 9th AMS annual meeting*, pp 1–16, New Orleans, LA, USA
- Straus PR (1999) Correcting GPS occultation measurements for ionospheric horizontal gradients. In: *Proceedings of ionospheric effects symposium*, Alexandria, VA, June
- Tricomi FG (1985) *Integral equations*. Dover, Mineola, New York, p 238
- Tsai L-C, Tsai WH (2004) Improvement of GPS/MET ionospheric profiling and validation with Chung-Li ionosonde measurements and the IRI. *Terr Atmos Ocean Sci* 15(4):589–607
- Tsai L-C, Liu CH, Hsiao TY, Huang JY (2009) A near real-time phenomenological model of ionospheric electron density based on GPS radio occultation data. *Radio Sci* 44. doi:[10.1029/2009RS004154](https://doi.org/10.1029/2009RS004154)
- Tsai L-C, Kevin Chang K, Liu CH (2011) GPS radio occultation measurements on ionospheric electron density from low Earth orbit. *J Geodesy*. doi:[10.1007/s00190-011-0476-9](https://doi.org/10.1007/s00190-011-0476-9)
- Tsai L-C, Macalalad EP, Liu CH (2014a) TaiWan Ionospheric Model (TWIM) prediction based on time series autoregressive analysis. *Radio Sci* 49. doi:[10.1002/2014RS005448](https://doi.org/10.1002/2014RS005448)
- Tsai L-C, Tien MH, Chen GH, Zhang Y (2014b) HF radio angle-of-arrival measurements and ionosonde positioning. *Terr Atmos Ocean Sci* 25:401–413. doi:[10.3319/TAO.2013.12.19.01\(AA\)](https://doi.org/10.3319/TAO.2013.12.19.01(AA))
- Tulasi Ram, S, Su S-Y, Liu CH (2009) FORMOSAT-3/COSMIC observations of seasonal and longitudinal variations of equatorial ionization anomaly and its interhemispheric asymmetry during the solar minimum period. *J Geophys Res* 114:A06311. doi:[10.1029/2008JA013880](https://doi.org/10.1029/2008JA013880)
- Wu X, Hu X, Gong X, Zhang X, Wang X (2009) An asymmetry correction method for ionospheric radio occultation. *J Geophys Res* 114:A03304. doi:[10.1029/2008JA013025](https://doi.org/10.1029/2008JA013025)

Yue X, Schreiner WS, Kuo Y-H (2012) A feasibility study of the radio occultation electron density retrieval aided by a global ionospheric data assimilation model. *J Geophys Res* 117(A08301). doi:[10.1029/2011JA017446](https://doi.org/10.1029/2011JA017446)

Yue X, Schreiner WS, Pedatella N, Anthes RA, Mannucci AJ, Straus PR, Liu JY (2014) Space weather observations by GNSS radio occultation: from FORMOSAT-3/COSMIC to FORMOSAT-7/COSMIC-2. *Space Weather* 12. doi:[10.1002/2014SW001133](https://doi.org/10.1002/2014SW001133)